Raman Spectroscopy of Carbon Nanotubes in 1997 and 2007†

M. S. Dresselhaus,*,‡ G. Dresselhaus,§ and A. Jorio||

Department of Physics and Department of Electrical Engineering and Computer Science, Massachusetts Institute of Technology, Cambridge, Massachusetts 02139, Francis Bitter Magnet Lab, Massachusetts Institute of Technology, Cambridge, Massachusetts 02139, and Departamento de Física, Universidade Federal de Minas Gerais, Belo Horizonte-MG, 30123-970, Brazil

Received: February 18, 2007; In Final Form: July 11, 2007

Over the last 10 years, carbon nanotubes have offered a unique system for the study of Raman spectra in one-dimensional systems, and at the same time Raman spectroscopy has provided a widely used and powerful tool for the characterization of single walled carbon nanotubes (SWNTs). The 10 year history of Raman scattering in SWNTs is reviewed here and future prospects for the field are discussed.

1. Introduction

The year 2007 marks 10 years since the first publication on Raman scattering in single wall carbon nanotubes (SWNTs) in 1997.[1] In the present article we review the 10 year history of this topic and discuss prospects for the future of the field.

The initial motivation for these Raman studies was two-fold: to examine the special characteristics of the Raman scattering process for a one-dimensional (1D) system and to use this technique to characterize the unique properties of carbon nanotubes. In fact, as we look back at the 10 year history of this field, both of these research directions have been strongly pursued.

Even though the diameter of a carbon nanotube is much smaller than the wavelength of light and the scattering volume is therefore exceptionally small, the use of Raman spectroscopy to characterize carbon materials generally[2] motivated researchers to apply this technique also to SWNTs shortly after the early synthesis of SWNTs in 1993.[3,4] Even though only ~1% of the carbonaceous material was estimated to be due to SWNTs in the sample used in the 1994 experiments,[5] a unique Raman spectrum was observed, namely, a double peak G-band structure, different from any other previously observed spectrum for a carbon material, thereby motivating further development of this noninvasive characterization technique for SWNTs.

Thus, when Smalley's group developed a laser ablation technique in 1996 to synthesize large enough quantities of high purity SWNT material[6] for a definitive Raman study of SWNTs, the early demonstration in 1994 that SWNTs had a unique Raman spectrum encouraged a collaboration to develop between the Smalley group at Rice University, the Eklund group at the University of Kentucky, and the Dresselhaus group at MIT. This collaboration resulted in the 1997 study of the Raman effect in SWNTs that opened up this field of investigation.[1] It should be mentioned that the generosity of Richard Smalley to share his precious samples with many research groups worldwide enabled many pioneering studies on SWNTs to occur, and these collaborations had a large impact on the early development of the science and applications of carbon nanotubes.

2. First Phase Raman Explorations

The first phase explorations of Raman spectroscopy on SWNTs spanned the 4 year period 1997−2001. Figure 1a taken from the 1997 paper that opened up this field[1] gives a general view of the Raman spectra from a typical SWNT bundle sample taken with five different laser excitation lines (E_{laser}). There are two dominant Raman signatures in these Raman spectra that distinguish a SWNT from other forms of carbon. The first relates to the low-frequency feature, usually in the range 100−300 cm^{-1}, arising from scattering by the radial breathing modes (RBM) which correspond to symmetric in-phase displacements of all the carbon atoms in the SWNT in the radial direction. The second signature relates to the multicomponent higher frequency features (around 1500−1600 cm^{-1}) associated with the tangential (G band) vibrational modes of SWNTs and is related to the Raman-allowed feature appearing in Raman spectra for graphite. Neither the RBM feature nor the multi-component G band features are observed in any other sp^2 bonded carbon material. Typically, sp^2 bonded carbon materials show a characteristic single G band (Lorentzian shape) Raman peak at about 1582 cm^{-1}. These two first-order Raman features (the RBM and the multi G-band) are, therefore, the spectral signatures of SWNTs and have been used to characterize nanotube samples from their earliest stage of identification.[5,8]

The unique optical properties observed in SWNTs are due to quantum confinement of their electronic states in the two directions perpendicular to the nanotube axis, resulting in so-called van Hove singularities (vHSs) in the nanotube density of states (DOS)[9,10] and to the strong many-body (electron−electron and electron−hole) excitonic effects.[11] These singularities in the DOS, and correspondingly in the joint density of states (JDOS) for optical transitions, are of great relevance for a variety of optical phenomena. Whenever the energy of the incident photons matches an optical transition energy (subject to selection rules for optical transitions), one expects to find resonant enhancement of the corresponding photophysical process. The resulting enhancement of the Raman intensity is known as the resonance Raman effect and this effect is especially strong in 1D systems.[12] Because of the sharpness of

† Part of the special issue "Richard E. Smalley Memorial Issue".

* Corresponding author.

‡ Department of Physics and Department of Electrical Engineering and Computer Science.

§ Francis Bitter Magnet Lab.

|| Universidade Federal de Minas Gerais.

10.1021/jp071378n CCC: $37.00
Published on Web 10/02/2007 PAGE EST: 6.4

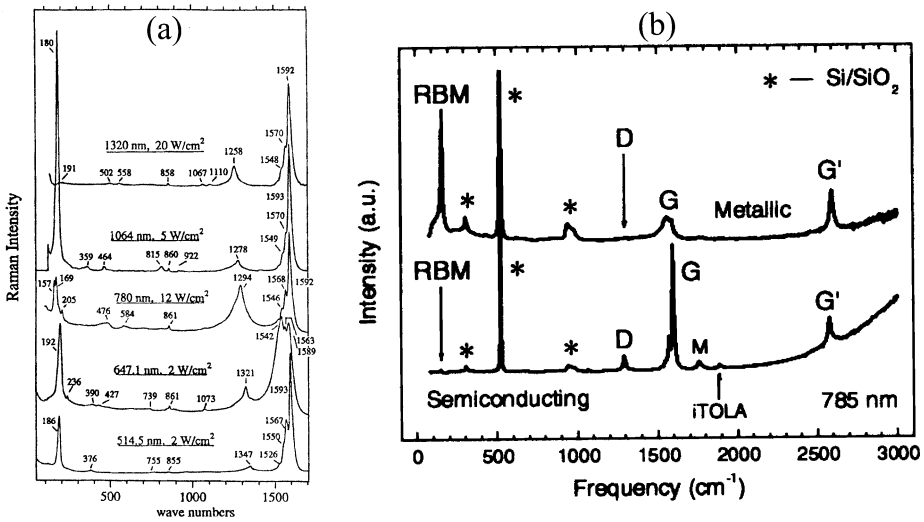

Figure 1. (a) Room-temperature Raman spectra from SWNT bundles grown by the laser vaporization method, excited at five different laser energies (wavelengths),[1] as indicated along with the power density and the vibrational frequencies (in cm^{-1}). From Rao et al. *Science* **1997**, *275*, 187−191. Reprinted with permission from AAAS. www.sciencemag.org. (b) Raman spectra from a metallic (top) and a semiconducting (bottom) SWNT at the single nanotube level. The dominant spectral features are indicated and are discussed in this manuscript. The Raman features denoted by ∗ come from the Si/SiO_2 substrate on which the nanotube is mounted.[7]

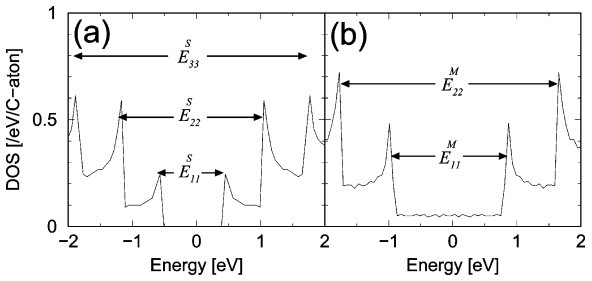

Figure 2. Electronic density of states for (a) a semiconducting SWNT and (b) a metallic SWNT. The Fermi energy (E_F) is located at $E = 0$. An optical transition is possible between vHS peaks in the valence and conduction bands. Energy separations between two vHS peaks are labeled from smallest to largest for semiconducting (S) tubes by E_{11}^S, E_{22}^S, E_{33}^S, ..., and for metallic (M) tubes by E_{11}^M, E_{22}^M, ...

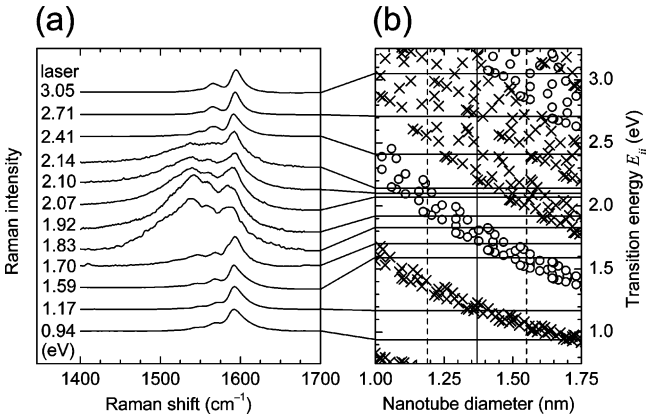

Figure 3. (a) Raman spectra of the tangential G-band modes of SWNT bundles measured with several different laser lines, on a sample with $d_t = 1.37 \pm 0.18$ nm.[13] (b) Resonant transition energies E_{ii} vs d_t. The vertical solid line is the average d_t and the vertical dashed lines denote the d_t distribution width. Crosses are for S SWNTs and open circles for M SWNTs.

these singularities, optical spectra can be strongly confined in energy, so that the optical spectra from SWNTs show sharp spectral features, similar to what is seen from single molecules, yet also showing behavior related to the quasi-continuum of states along the SWNT axis. Furthermore, because the (*n*, *m*) values of a SWNT are directly related to the SWNT diameter and chirality, the Raman spectra can distinguish one (*n*, *m*) SWNT from another by its diameter and chirality. For the case of SWNTs, each (*n*, *m*) nanotube has a unique set of energies in the conduction and valence bands where these vHSs occur (see Figure 2). This makes the resonance Raman effect for nanotubes selective of particular (*n*, *m*) SWNTs that are in resonance with E_{laser}. The fact that the spectra taken for different laser excitation energies differ from one another is associated with the resonance Raman effect, and the fact that each (*n*, *m*) nanotube has a different set of electronic resonance levels, so that each laser line accesses a different set of nanotubes. Since the number of atoms around the circumference of a tube is proportional to the nanotube diameter, it is expected that the frequency of the RBM mode ω_{RBM} will depend on the inverse tube diameter, as is observed experimentally.[9]

It was Smalley's hope that there would be one dominant (*n*, *m*) species in the nanotube samples grown by laser ablation and he expected the (10, 10) tubes to be the dominant species. The first Raman paper in 1997[1] showed this not to be the case. Thus the characterization of SWNT samples for their content of each (*n*, *m*) tube type was identified as an important goal and control of (*n*, *m*) in the growth process became a dominant goal of synthesis strategies. This topic is further discussed in section 5 in connection with nanotube metrology.

Soon after the discovery of the resonance Raman effect in SWNTs,[1] it was found that the line shape for the lower frequency G-band feature for metallic (M) tubes was broader, followed a Breit−Wigner−Fano line shape, and was down-shifted in frequency from semiconducting (S) tubes of similar diameter (see Figure 3).[13] This finding was important for using the Raman effect to distinguish between metallic and semiconducting tubes in typical nanotube bundles which contained both semiconducting and metallic tubes. Advances in the synthesis of carbon nanotubes also took place in the 1997−2001 time frame allowing the use of catalyzed chemical vapor (CVD) techniques in the growth of samples of isolated individual SWNTs on an insulating substrate, such as oxidized silicon (Si/SiO_2).[14] Furthermore, surface enhanced Raman spectra (SERS) of carbon nanotubes[15] suggested that it might be possible to observe Raman spectra from a single individual SWNT, thus launching the field into its second phase of activity, which was

focused on the observation of Raman spectra from a single individual (n, m) SWNT.

3. Second Phase Explorations

The second phase explorations of Raman spectroscopy on SWNTs was opened by the observation of Raman spectra from a single nanotube,[7] as shown in Figure 1b, for both a semiconducting and a metallic nanotube.

Observations at the single nanotube level allowed observation of the dependence on diameter and chirality of each feature in the Raman spectra for SWNTs shown in Figure 1b. Such studies furthermore advanced our understanding of Raman spectroscopy in 1D materials generally, since SWNT properties could now be measured in great detail at the single nanotube level from an object only ~1 nm in diameter with a well-defined geometrical structure.[7]

For SWNTs, the energy separation which is relevant to resonance Raman spectroscopy corresponds to the optical transition energies E_{ii} discussed above. Because of quantum confinement effects, the electronic structure of an (n, m) SWNT has many vHSs (see Figure 2). However, despite the large number of vHSs, only a small number of electronic levels can be connected through the electromagnetic interaction associated with the incident light due to symmetry selection rules. Electrons (and phonons) in carbon nanotubes are characterized by their wave vectors along the nanotube axis (k for electrons and q for phonons) and by their symmetries.[9] It is known that light can be strongly absorbed when the polarization of the electric field is parallel to the nanotube axis.[9] In this case, valence and conduction electrons having the same sub-band or cutting line index i so that the electronic states ($E_i^{\mathrm{v}} \rightarrow E_i^{\mathrm{c}}$) are coupled by light polarized parallel to the nanotube axis.[9]

Because of selection rule considerations,[9,16] optical transitions normally occur between peak i in the valence band to peak i in the conduction band (see Figure 2, subject to excitonic and other many body effects).[12] These transitions are labeled E_{11}, E_{22}, E_{33}, and so on, in order of increasing energy, with E_{11} having the smallest energy. Each (n, m) carbon nanotube has a unique set of E_{ii} values. We further note in Figure 2, that the DOS at E_{F} for metallic tubes is nonzero and constant between the highest valence band vHS and the lowest conduction band vHS.

The actual transition energies E_{ii} are excitonic in nature because the excited electron is bound to the hole that is left behind in the excitation process, giving rise to what is called a bound electron−hole pair or an exciton. The actual E_{ii} are further perturbed by electron−electron repulsion effects, and it is the combination of these attractive and repulsive interactions that give rise to the optical transition energies E_{ii} that are observed experimentally and calculated theoretically. These electron−hole and electron−electron interactions are specially strong in 1D systems, since the electrons and holes are highly confined in 1D space. This topic is further discussed in section 4.

To analyze the resonance Raman spectra of SWNTs, it is useful to have a plot of these resonant transition energies E_{ii} as a function of tube diameter d_{t} for all (n, m) SWNTs, and we call such a plot a Kataura plot (see Figure 4).[17−19]

From the Kataura plot in Figure 4, we see that the resonant transition energies E_{ii} are approximately inversely proportional to d_{t}, and each E_{ii} band in Figure 4 has some width due to the chirality (d_{t}, θ) dependence of E_{ii}.[20] For a given d_{t}, the sequence of E_{ii} is in the order E_{11}^{S}, E_{22}^{S}, E_{11}^{M}, E_{33}^{S}, etc. starting from the lowest energy, where the superscripts M and S refer to metallic and semiconducting SWNTs. From the Kataura plot in Figure 4, we see, for example, that for a sample with a diameter distribution of $d_{\mathrm{t}} = 1.4 \pm 0.1$ nm, a Raman signal from semiconducting (S) and metallic (M) SWNTs would be expected to occur for $E_{\mathrm{laser}} \sim 1.4$ eV (E_{22}^{S}) and 1.9 eV (E_{11}^{M}), respectively.

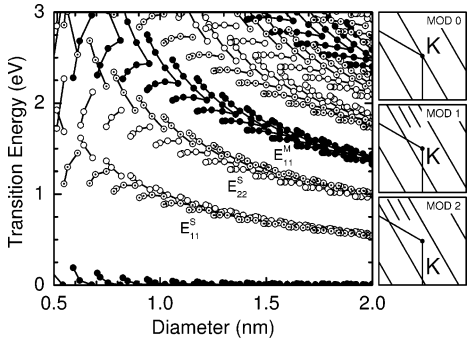

Figure 4. Plot of the transition energies E_{ii} vs d_{t} for all (n, m) values occurring for $0.5 < d_{\mathrm{t}} < 2.0$ nm (Kataura plot) where S and M denote semiconducting and metallic nanotubes, respectively. On the right, cutting lines are shown for M tubes (MOD0), and S tubes of two types (MOD1 and MOD2) for ○ and ⊙. The short parallel lines for the two lower figures on the right indicate that the K point is located $^1/_3$ or $^2/_3$ of the distance between cutting lines for S tubes and is located on a cutting line for M tubes.

Measurements of the frequency of the radial breathing mode and the resonant energy E_{ii} at the single nanotube level allow a determination to be made of the d_{t} and nanotube chirality θ of a specific (n, m) SWNT.[9] An expression for the relation between the radial breathing mode frequency ω_{RBM} and the diameter that is in current usage is given by eq 1 in section 5. In addition, single nanotube spectroscopy allows measurements to be made of the resonant window of an individual SWNT, if a suitable tunable laser system such as a Ti:sapphire laser or a dye laser system is available.[21]

Once the (n, m) of a given tube is identified, then the dependence of the frequency and intensity of each of the features in the Raman spectra (see Figure 1b) on diameter and chiral angle can be found, including the RBM, G-band, D-band, G′-band, and various overtone and combination modes within the first order and higher order frequency regions. Such studies have played a major role in advancing the fundamental understanding of Raman spectroscopy for 1D systems and in characterizing actual SWNT samples.[12] The (n, m) tube characterization, when used in conjunction with studies on the D-band and G′-band optical spectra (which have a large dispersion with laser excitation energy), allow measurements to be made for both electrons and phonons with wave vectors away from the K point. Such measurements have enabled experimental studies to be made of the trigonal warping effect for both the electronic and phonon dispersion relations. The (n, m) identification enabled by single molecule Raman spectroscopy allowed measurement of transport, strain, and other physical properties at the single nanotube level while determining the dependence of these physical properties on the nanotube diameter and chiral angle.

Furthermore, the idea that the large enhancement factor provided by the 1D density of states where the laser energy is in resonance with a quantized electronic state of the nanotube stimulated the development of other complementary and powerful optical techniques with the ability to do (n, m) SWNT identification. Examples of such techniques are photoluminescence[22] and Rayleigh scattering.[23] The availability of these multiple powerful optical techniques has launched us into the present phase of the Raman exploration of carbon nanotubes.

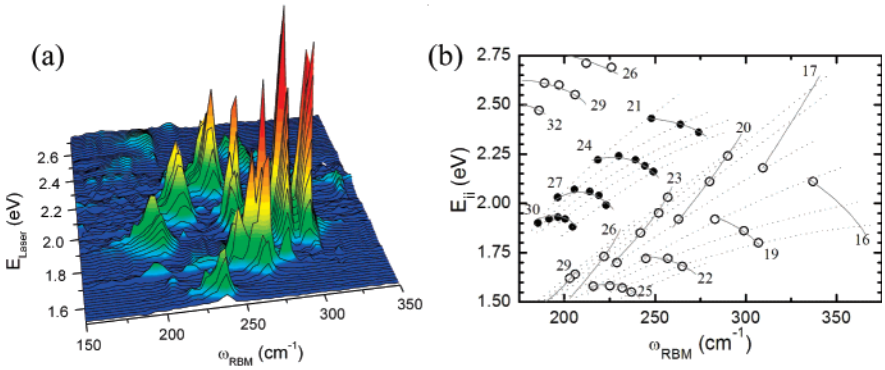

Figure 5. (a) RBM resonance Raman measurements of HiPco SWNT nanotubes, wrapped in SDS and dispersed in an aqueous solution,[25] taken with 76 different laser lines E_{laser} between 1.52 and 2.71 eV.[27] (b) The points denote 47 electronic transition energies E_{ii} vs ω_{RBM} for 41 different (n, m) SWNTs in part a. ● and ○, respectively, denote metallic and semiconducting SWNTs. Each family is denoted by its ($2n + m$) = constant value, allowing family patterns to be clearly seen.

4. Present Status

The present phase of Raman studies in SWNTs was initiated by the demonstration of photoluminescence from individual carbon nanotubes[24] wrapped in sodium dodecyl sulfate (SDS) to separate one SWNT from another so that the SWNT could reside in an excited-state long enough to luminesce. In these experiments, the excitation is typically made at the transition energy E_{22}^S and the emission is typically observed at E_{11}^S. The results from the photoluminescence experiments are typically presented in terms of a plot of the resulting E_{11}^S vs E_{22}^S energies for all the (n, m) semiconducting tubes in the sample. From analysis of systematic patterns in the observed data it was possible to make an identification of each transition energy E_{ii}^S with specific (n, m) tubes.[12,25,26] This work raised two serious challenges to the Raman characterization of (n, m) for SWNTs. The first challenge, was that the E_{ii}^S values obtained from photoluminescence (PL) did not initially seem to be consistent with E_{ii}^S values obtained by resonance Raman spectroscopy (RRS). The second challenge was that the data points obtained in a Kataura plot based on the PL measurements showed family behavior, strong departures from the tight binding model previously used to interpret RRS behavior, including a strong departure from the "ratio rule" of $E_{22}^S/E_{11}^S = 2$. These issues broke the RRS field for SWNTs wide open when addressed, resulting in several new research directions.

The first challenge was met by developing a Raman experimental system with many laser lines, so that it would be possible to obtain the E_{ii} energies for many tubes, as shown in Figure 5a where Raman intensity contours vs ω_{RBM} are shown. These data were obtained from resonance Raman spectra[27] taken from a HiPco sample (a CVD grown sample from high purity CO gas) with a diameter distribution $d_t = 1.0 \pm 0.3$ nm where the individual tubes were wrapped with SDS (sodium dodecyl sulfate).[25] The same sample was chosen for both PL and RRS experiments.[27]

In order to avoid use of an empirical fitting procedure in implementing the Kataura plot, we plot E_{ii} vs ω_{RBM} (Figure 5b) directly from the experimental values in Figure 5a for each (n, m) resonant SWNT.[27] ● and ○ represent, respectively, M and S SWNTs. Using 76 values of E_{laser} for $1.52 \leq E_{laser} \leq 2.71$ eV, a 2D plot is made from the RBM spectra obtained from Stokes resonance Raman measurements as a function of E_{laser}. Each RBM peak in Figure 5a can be assigned to a (n, m) SWNT with the idea of family patterns introduced by the PL experiments. The family patterns of E_{ii} ($2n + m$ = constant) for semiconducting (E_{22}^S and E_{33}^S) and metallic (E_{11}^M) tubes are clearly seen in Figure 5b, where we also show the values of ($2n + m$), corresponding to tubes with approximately the same tube diameter d_t. The different behaviors of the MOD1 and MOD2 semiconducting SWNTs in the Kataura plot are clearly seen, where for semiconducting SWNTs we distinguish the case where the remainder of the division of ($2n + m$)/3 is 1 or 2 by MOD1 (○) and MOD2 (⊙), in Figure 4, respectively. We thus see that the energies E_{ii}^S follow a similar pattern (the so-called family behavior), according to the $2n + m$ value of a SWNT (which labels its family) and whether the SWNT is MOD1 or MOD2.[26,28] Thus, a (6, 5) SWNT would be designated by MOD2 and family $2n + m = 17$. Each metallic SWNT has two van Hove singularities in its DOS for each E_{ii}^M, except for armchair SWNTs. The occurrence of two vHSs for each E_{ii}^M is due to the so-called trigonal warping effect of the electronic structure,[20] and the energy separation between the two vHSs for a metallic tube generally increases as the chiral angle decreases. Family patterns are observed in Figure 4 for both S and M SWNTs.

The (E_{ii}, ω_{RBM}) results extracted from analysis of Figure 5a are plotted in Figure 5b. These (E_{ii}, ω_{RBM}) results were compared with the extended tight binding (ETB) theoretical model that considers in detail the distortion of the C−C bonds due to the curvature of the graphene sheet when it is rolled up to form a SWNT.[18,29] The model also considers the effects of the excitonic binding of the excited electron−hole pair and the Coulomb repulsion of electrons, and when the model is compared with the RRS experimental results a clear (n, m) assignment for each tube is obtained.

Of particular importance is the fact that a comparison between RRS and PL measurements yields good agreement between the E_{ii}^S values obtained when the same nanotube sample is used for both RRS and PL measurements. Another practical outcome of this effort was to show that Raman spectroscopy using many laser lines is necessary to make three-dimensional (3D) Kataura-like density maps which include intensity contours as is commonly done in photoluminescence. Thus a new standard for data presentation of RRS data in terms of these 3D Kataura plots, and plots of Raman intensity and frequency along the nanotube position has become common practice. It should be noted that whereas PL can only characterize semiconducting (S) SWNTs, RRS can characterize both S and M SWNTs.

The departure from the ratio rule of $E_{22}^S/E_{11}^S = 2$ for armchair tubes, as predicted by the tight binding model, has led to much more sophisticated first principles models for treating many body effects in 1D systems and has led to the

extended tight-binding (ETB) model used for Figure 5b which is suitable for the calculation of a Kataura plot that includes many small diameter SWNTs. Current RRS and PL experiments on carbon nanotubes are now explained in terms of a many-body excitonic picture. Because of the special symmetry of the K point in the graphene Brillouin zone, there are in fact four different excitonic states but only one of these is Raman active. Thus, the Kataura plots that have been used so successfully to explain experimental results in the past can now be taken over to the excitonic picture upon which the $2n + m =$ constant family effects observed in Figure 5 must be carefully considered.

5. The Next Phase of Exploration

The next phase of exploration of the Raman spectroscopy of carbon nanotubes is likely to include a number of topics identified below. First, we can expect to have a major focus devoted to directing the technique to applications, which will require the development of carbon nanotube metrology. The rapid development of nanotube science and applications urges studies on metrology, standardization, and industrial quality control.[30−33] The development of protocols for the definition of sample parameters like structural metrics (carbon−carbon distance, diameter, chiral angle, surface area), physical properties (optical, thermal, mechanical), composition (impurity content, purity of SWNTs relative to DWNTs and MWNTs, spatial homogeneity), and stability (dispersability, biocompatibility, and health effects) are important for both research and applications of nanotubes. These protocols are expected to be applicable not only to carbon nanotubes but also to the exploding field of nanomaterials, where metrology issues will drive technological growth and innovation. Nanoscience promises a revolution in technology, bringing us back to the very basic problem of defining metrics and measurement systems, and ultimately back to the fundamentals of metrology for samples of nanoscale size, for which the properties and measurement systems differ from bulk systems. That is to say, the characterization of a sample 1 μm in size and 1 nm in size will require different measurement strategies, because in the nanoscale regime, length scale itself becomes a parameter describing the properties of a material.

Different from STM and TEM related techniques, optics is one of the oldest characterization techniques for materials science, being largely used long before nanoscience could even be imagined. Optical techniques, especially optical absorption, resonance Raman spectroscopy, and photoluminescence, have been largely used to characterize carbon nanotubes. The advantages of optics relate to both experimental considerations and fundamental aspects. Experimentally, the techniques are readily available, relatively simple to perform, quick, and can be performed at room temperature and under ambient pressure. Fundamentally, the optical techniques (normally with visible wavelengths) are nondestructive and noninvasive because they use the photon, a massless and chargeless particle, as a probe. Furthermore, optical experiments can be carried out at the single nanotube level[7] due to the unusually high optical response of the nanotubes, which in turn is a consequence of the one-dimensional confinement of their electronic structure.[34]

Raman spectroscopy has been commonly used for characterizing SWNTs because it is one of the most sensitive characterization tools for these nanostructures.[35,36] For example, the RBM has the very important property of being related to the tube diameter. By considering that common Raman systems have a spectral accuracy of about 1 cm^{-1} and that the RBM frequencies (ω_{RBM}) from nanotube samples (with diameters d_t from 0.5 to 5.0 nm) range from 50−500 cm^{-1}, Raman spectroscopy can determine the tube diameter with an accuracy of up to 0.2%. This means that the diameter for a 5.0 nm tube can be found to an accuracy of 0.1 nm, with the accuracy increasing with decreasing diameter, reaching an accuracy of 0.01 nm, for a $d_t = 0.5$ nm tube. However, the big problem is the determination of the precise relation between ω_{RBM} and d_t. For smaller diameter tubes, where the accuracy in measuring ω_{RBM} is larger, ω_{RBM} is expected to also show a small dependence on the chiral angle θ. The smaller the tube diameter, the larger the curvature effects that induce θ dependent variations in the a_{C-C} bond lengths.

Although the RBM frequency has been shown to be weakly dependent on doping (charge transfer) or laser heating, there are a large number of different ω_{RBM} vs d_t relations in the literature. Simple force constant calculations predict a linear dependence between ω_{RBM} and the inverse diameter ($1/d_t$), and this has been confirmed experimentally within certain regimes. The expected fundamental relation is $\omega_{RBM} = 227/d_t$ (ref 29), however, when considering low diameter samples (d_t below 1.4 nm), the relation between ω_{RBM} and d_t has converged to[37]

$$\omega_{RBM} = (219 \pm 3)/d_t + (15 \mp 3) \quad (1)$$

with some evidence for a θ dependence on the order of 3 cm^{-1} and for a dependence on whether the tube is semiconducting or metallic, probably related to the constant factor in the ω_{RBM} vs d_t relation. This constant term was initially supposed to be a bundling effect, but its origin is still not clear from a fundamental standpoint.

In the large diameter limit ($d_t > 1.4$ nm) different relations have been obtained, suggesting a nonuniversal $1/d_t$ dependence for ω_{RBM}. The (n, m) dependence for the RBM frequency is, therefore, still not completely established, and there is still room for developing a metrology for more accurately determining SWNT diameters. The natural RBM linewidth (γ_{RBM}) has been established as 3 cm^{-1} for isolated SWNTs on Si/SiO_2 substrates.[38] A d_t dependence on γ_{RBM} has been observed, showing that for larger diameter tubes (above 3 nm) the RBM feature gets too broad and cannot be observed. This characteristic thus limits the use of the RBM feature to study large diameter multiwall carbon nanotubes. The RBM from MWNTs is only observed when they have very small diameter inner tubes (below 3 nm).

Finally, analysis of the RBM resonance profiles (RBM intensity as a function of E_{laser}) can be used to measure the E_{ii} for specific (n, m) tubes whether they are within bundles, isolated in aqueous solution, or on Si substrates. Since (E_{laser}, ω_{RBM}) and (E_{ii}, $1/d_t$) can be directly related, the plot of E_{laser} vs ω_{RBM} is a direct measure of the Kataura plot displayed as a function of $1/d_t$. Such a plot can therefore be used to measure the effect of temperature, pressure, bundling, etc. on the E_{ii} optical levels. The resonance profile linewidth (Γ_r) ranges from 8 meV for isolated tubes on a Si substrate up to 160 meV for SWNTs in bundles, giving information about the interactions of SWNTs with their environments. The intensity analysis furthermore gives the (n, m) dependent population of SWNTs in a given sample.[33] The use of such a Raman experiment for the comparative analysis of SWNTs can be easily performed, but for an absolute (n, m) population assignment, the resonance Raman cross section dependence on (n, m) has to be established. Theory shows that the electron−phonon coupling[39] has a very strong (n, m) dependence on the overall theoretical predictions (like a larger Raman cross section is found for smaller chiral angle tubes or the tube type dependence arising from the mod-[$(2n + m)$, 3] dependence, both parameters changing the Raman

intensities by about 1 order of magnitude) and such effects have also been observed experimentally. However, theory still has to be fully validated for providing a trustworthy determination of each (*n*, *m*) population in carbon nanotube samples using resonance Raman spectroscopy. Again, measurements on isolated tubes might be necessary, although comparative analysis technique (such as Raman vs photoluminescence, Raman vs optical absorption) have shed considerable light into this problem.[40]

Another very important and very informative Raman feature that also requires more systematic work for achieving the full characterization capability of Raman spectroscopy in carbon materials is the disorder-induced feature, called the D band. The D band has been largely used for the characterization of carbon samples over many decades,[41] but mostly in a qualitative way. The D band is observed when there is a symmetry-breaking perturbation on the hexagonal sp^2 bonded lattices for graphite and nanotubes. The observation of a D band in the Raman spectra is, therefore, related to either the presence of defects in the tube walls (e.g., vacancies, 7-5 pairs, dopants, or just the tube ends) or to the presence of amorphous carbon material in the sample. The D band intensity was shown to increase by SWNT irradiation and by B doping[42,43] (both procedures inducing defects). Systematic work for defining metrics for the D band intensity has been developed with tube length shortening (the smaller the tube length, the more important the edge effects[44]). Near field Raman spectroscopy (spectral resolution 20 nm) shows that the D band scattering is localized along a single tube and the D band intensity profiles vary strongly among single tubes grown by different synthesis methods.[45] The D band intensity is expected to show even more sophisticated properties, like the dependence on the atomic edge structure that is observed in graphite edges.[46] Because of this strong potential for very sophisticated characterization of nanocarbons, more detailed theoretical and experimental studies of the D band problem are now taking place.

Major efforts are now taking place in controlling the synthesis of carbon nanotubes, and breakthroughs are expected in the coming years in the synthesis of the desired (*n*, *m*) nanotube, at the desired location, and growing in the desired direction and to the desired length. Raman spectroscopy is expected to play a major role in the detailed characterization of nanotubes thus produced. As nanotubes become more commercialized, it is expected that Raman spectroscopy will be developed into a metrological tool for the characterization of carbon nanotubes.

Acknowledgment. The authors wish to thank Richard Smalley for his contributions to launching early work on both Raman spectroscopy and photoluminescence studies of carbon nanotubes and for his continuing interest in the photophysics of carbon nanotubes toward advancing both science and applications for societal benefit. A.J. acknowledges financial support by Grants PRPq-UFMG, FAPEMIG, and CNPq, Brazil. G.D. and M.S.D. acknowledge support under NSF Grant DMR 04-05538.

References and Notes

(1) Rao, A. M.; Richter, E.; Bandow, S.; Chase, B.; Eklund, P. C.; Williams, K. W.; Fang, S.; Subbaswamy, K. R.; Menon, M.; Thess, A.; Smalley, R. E.; Dresselhaus, G.; Dresselhaus, M. S. Diameter-selective Raman scattering from vibrational modes in carbon nanotubes. *Science* **1997**, *275*, 187−191.

(2) Dresselhaus, M. S.; Dresselhaus, G.; Rao, A. M.; Jorio, A. A.; Souza Filho, G.; Samsonidze, G. G.; Saito, R. Resonant Raman scattering on one-dimensional systems. *Indian J. Phys.* **2003**, *77B*, 75−99.

(3) Iijima, S.; Ichihashi, T. Single shell carbon nanotubes of 1-nm diameter. *Nature* (*London*) **1993**, *363*, 603.

(4) Bethune, D. S.; Kiang, C. H.; de Vries, M. S.; Gorman, G.; Savoy, R.; Vazquez, J.; Beyers, R. Cobalt-catalysed growth of carbon nanotubes with single atomic layer walls. *Nature* (*London*) **1993**, *363*, 605.

(5) Holden, J. M.; Zhou, P.; Bi, X. X.; Eklund, P. C.; Bandow, S.; Jishi, R. A.; Chowdhury, K. D.; Dresselhaus, G.; Dresselhaus, M. S. Raman scattering from nanoscale carbons generated in a cobalt-catalyzed carbon plasma. *Chem. Phys. Lett.* **1994**, *220*, 186−191.

(6) Thess, A.; Lee, R.; Nikolaev, P.; Dai, H.; Petit, P.; Robert, J.; Xu, C.; Lee, Y. H.; Kim, S. G.; Rinzler, A. G.; Colbert, D. T.; Scuseria, G. E.; Tománek, D.; Fischer, J. E.; Smalley, R. E. Crystalline ropes of metallic carbon nanotubes. *Science* **1996**, *273*, 483−487.

(7) Jorio, A.; Saito, R.; Hafner, J. H.; Lieber, C. M.; Hunter, M.; McClure, T.; Dresselhaus, G.; Dresselhaus, M. S. Structural (*n*, *m*) determination of isolated single-wall carbon nanotubes by resonant Raman scattering. *Phys. Rev. Lett.* **2001**, *86*, 1118−1121.

(8) Tohji, K.; Goto, T.; Takahashi, H.; Shinoda, Y.; Shimizu, N.; Jeyadevan, B.; Matsuoka, I.; Saito, Y.; Kasuya, A.; Ohsuna, T.; Hiraga, K.; Nishina, Y. Purifying single walled nanotubes. *Nature* **1996**, *383*, 679.

(9) Saito, R.; Dresselhaus, G.; Dresselhaus, M. S. *Physical Properties of Carbon Nanotubes*; Imperial College Press: London, 1998.

(10) Dresselhaus, M. S., Dresselhaus, G., Avouris, P., Eds. *Carbon Nanotubes: Synthesis, Structure, Properties and Applications*; Topics in Applied Physics; Springer-Verlag: Berlin, Germany, 2001; Vol. 80.

(11) Dresselhaus, M. S.; Dresselhaus, G.; Saito, R.; Jorio, A. Exciton photophysics of carbon nanotubes. In *Annual Reviews of Physical Chemistry Chemical Physics*; Leone, S. R., Groves, J. T., Ismagilov, R. F., Richmond, G., Eds.; Intelligent Synthesis of the Scientific Literature: Palo Alto, CA, 2007; Vol. 58, pp 719−747.

(12) Dresselhaus, M. S.; Dresselhaus, G.; Saito, R.; Jorio, A. Raman spectroscopy of carbon nanotubes. *Phys. Rep.* **2005**, *409*, 47−99.

(13) Pimenta, M. A.; Marucci, A.; Empedocles, S.; Bawendi, M.; Hanlon, E. B.; Rao, A. M.; Eklund, P. C.; Smalley, R. E.; Dresselhaus, G.; Dresselhaus, M. S. Raman modes of metallic carbon nanotubes. *Phys. Rev. B* **1998**, *58*, R16016−R16019.

(14) Liu, J.; Fan, S.; Dai, H. Recent advances in methods of forming carbon nanotubes. *MRS Bull.* 2004, 29, 244−250.

(15) Kneipp, K.; Kneipp, H.; Corio, P.; Brown, S. D. M.; Shafer, K.; Motz, J.; Perelman, L. T.; Hanlon, E. B.; Marucci, A.; Dresselhaus, G.; Dresselhaus, M. S. Surface-enhanced and normal stokes and anti-stokes Raman spectroscopy of single-walled carbon nanotubes. *Phys. Rev. Lett.* **2000**, *84*, 3470−3473.

(16) Ajiki, H.; Ando, T. Physics of carbon nanotubes. *Physica B* **1994**, *201*, 349.

(17) Kataura, H.; Kumazawa, Y.; Kojima, N.; Maniwa, Y.; Umezu, I.; Masubuchi, S.; Kazama, S.; Zhao, X.; Ando, Y.; Ohtsuka, Y.; Suzuki, S.; Achiba, Y. Optical absorption and resonant Raman scattering of carbon nanotubes. In *Electronic Properties of Novel Materials-Science and Technology of Molecular Nanostructures*, Proceedings of the XIII International Winter School on Electronic Properties of Novel Materials (IWEPNM'99) 486, Kirchberg, Tyrol, Austria, February 27−March 6, 1999; Kuzmany, H., Mehring, M., Fink, J., Roth, S., Eds.; American Institute of Physics: Woodbury, NY, 1999; pp 328−332.

(18) Samsonidze, G. G.; Saito, R.; Kobayashi, N.; Grüneis, A.; Jiang, J.; Jorio, A.; Chou, S. G.; Dresselhaus, G.; Dresselhaus, M. S. Family behavior of the optical transition energies in single-wall carbon nanotubes of smaller diameters. *Appl. Phys. Lett.* **2004**, *85*, 5703−5705.

(19) Popov, V. N.; Henrard, L.; Lambin, P. Resonant Raman intensity of the radial breathing mode of single-walled carbon nanotubes within a non-orthogonal tight-binding model. *Nano Lett.* **2004**, *4*, 1795−1799.

(20) Saito, R.; Dresselhaus, G.; Dresselhaus, M. S. Trigonal warping effect of carbon nanotubes. *Phys. Rev. B* **2000**, *61*, 2981−2990.

(21) Jorio, A.; Souza Filho, A. G.; Dresselhaus, G.; Dresselhaus, M. S.; Saito, R.; Hafner, J. H.; Lieber, C. M.; Matinaga, F. M.; Dantas, M. S. S.; Pimenta, M. A. Joint density of electronic states for one isolated single-wall carbon nanotube studied by resonant Raman scattering. *Phys. Rev. B* **2001**, *63*, 245416..

(22) Lefebvre, J.; Fraser, J.; Finnie, P.; Homma, Y. Photoluminescence from an individual single-walled carbon nanotube. *Phys. Rev. B* **2004**, *69*, 075403.

(23) Bottani, C. E.; Bassi, A. L.; Beghi, M. G.; Podesta, A.; Milani, P.; Zakhidov, A.; Baughman, R.; Walters, D. A.; Smalley, R. E. Dynamic light scattering from acoustic modes in single-walled carbon nanotubes. *Phys. Rev. Lett.* (2003).

(24) Barros, E. B.; Jorio, A.; Samsonidze, G. G.; Capaz, R. B.; Filho, A. G.; Filho, J. M.; Dresselhaus, G.; Dresselhaus, M. S. Review on the symmetry related properties of carbon nanotubes. *Phys. Rep.* **2006**, *431*, 261−302.

(25) O'Connell, M. J.; Bachilo, S. M.; Huffman, X. B.; Moore, V. C.; Strano, M. S.; Haroz, E. H.; Rialon, K. L.; Boul, P. J.; Noon, W. H.; Kittrell, C.; Ma, J.; Hauge, R. H.; Weisman, R. B.; Smalley, R. E. Band gap fluorescence from individual single walled carbon nanotubes. *Science* **2002**, *297*, 593−596.

(26) Bachilo, S. M.; Strano, M. S.; Kittrell, C.; Hauge, R. H.; Smalley, R. E.; Weisman, R. B. Structure-assigned optical spectra of single walled carbon nanotubes. *Science* **2002**, *298*, 2361−2366.

(27) Fantini, C.; Jorio, A.; Souza, M.; Strano, M. S.; Dresselhaus, M. S.; Pimenta, M. A. Optical transition energies for carbon nanotubes from resonant Raman spectroscopy: Environment and temperature effects. *Phys. Rev. Lett.* **2004**, *93*, 147406.

(28) Weisman, R. B.; Bachilo, S. M. Dependence of optical transition energies on structure for single-walled carbon nanotubes in aqueous suspension: An empirical Kataura plot. *Nano Lett.* **2003**, *3*, 1235−1238.

(29) Jorio, A.; Fantini, C.; Pimenta, M. A.; Capaz, R. B.; Samsonidze, G. G.; Dresselhaus, G.; Dresselhaus, M. S.; Jiang, J.; Kobayashi, N.; Grüneis, A.; Saito, R. Resonance Raman spectroscopy (*n*, *m*) dependent effects in small diameter single-wall carbon nanotubes. *Phys. Rev. B* **2005**, *71*, 075401.

(30) Rinzler, A. G.; Liu, J.; Dai, H.; Nikolaev, P.; Huffman, C. B.; Rodriguez-Marcias, F. J. Large scale purification of single-wall carbon nanotubes: process, product and characterization. *Appl. Phys. A* **1998**, *67*, 29−37.

(31) Chiang, I. W.; Brinson, B. E.; Smalley, R. E.; Margrave, J. L.; Hauge, R. H. Purification and characterization of single-wall carbon nanotubes. *J. Phys. Chem. B* **2001**, *105*, 1157−1161.

(32) Arepalli, S.; Nikolaev, P.; Gorelik, O.; Hadjiev, V. G.; Holmes, W.; Files, B.; Yowell, L. Protocol for the characterization of single-wall carbon nanotube material quality. *Carbon* **2004**, *42*, 1783−1791.

(33) Jorio, A.; Santos, A. P.; Ribeiro, H. B.; Fantini, C.; Souza, M.; Vieira, J. P. M.; Furtado, C. A.; Jiang, J.; Balzano, L.; Resasco, D. E.; Pimenta, M. A. Quantifying carbon-nanotube species with resonance Raman scattering. *Phys. Rev. B* **2005**, *72*, 075207..

(34) Jorio, A.; Saito, R.; Hertel, T.; Weisman, R. B.; Dresselhaus, G.; Dresselhaus, M. S. Carbon nanotube photophysics. *MRS Bull.* **2004**, *29*, 276−280.

(35) Dresselhaus, M. S.; Eklund, P. C. Phonons in carbon nanotubes. *Adv. Phys.* **2000**, *49*, 705−814.

(36) Jorio, A.; Pimenta, M. A.; Souza Filho, A. G.; Saito, R.; Dresselhaus, G.; Dresselhaus, M. S. Characterizing carbon nanotube samples with resonance Raman scattering. *New J. Phys.* **2003**, *5*, 1.1−1.17.

(37) Araujo, P. T.; Doorn, S. K.; Kilina, S.; Tretiak, S.; Einarsson, E.; Maruyama, S.; Chacham, H.; Pimenta, M. A.; Jorio, A. Third and fourth optical transitions in semiconducting carbon nanotubes. *Phys. Rev. Lett.* **2007**, *98*, 067401.

(38) Jorio, A.; Fantini, C.; Dantas, M. S. S.; Pimenta, M. A.; Souza Filho, A. G.; Samsonidze, G. G.; Brar, V. W.; Dresselhaus, G.; Dresselhaus, M. S.; Swan, A. K.; Ünlü, M. S.; Goldberg, B. B.; Saito, R. Linewidth of the Raman features of individual single-wall carbon nanotubes. *Phys. Rev. B* **2002**, *66*, 115411.

(39) Jiang, J.; Saito, R.; Samsonidze, G. G.; Jorio, A.; Chou, S. G.; Dresselhaus, G.; Dresselhaus, M. S. Chirality dependence of the exciton effects in single-wall carbon nanotubes. *Phys. Rev. B* **2007**, *75*, 035407.

(40) Jorio, A.; Fantini, C.; Pimenta, M. A.; Heller, D. A.; Strano, M. S.; Dresselhaus, M. S.; Oyama, Y.; Jiang, J.; Saito, R. Carbon nanotube population analysis from Raman and photoluminescence intensities. *Appl. Phys. Lett.* **2006**, *88*, 023109.

(41) Pimenta, M. A.; Dresselhaus, G.; Dresselhaus, M. S.; Cançado, L. G.; Jorio, A.; Saito, R. Studying disorder in graphite-based systems by Raman spectroscopy. *Phys. Chem. Chem. Phys.* **2007**, *9*, 1276−1290.

(42) Maultzsch, J.; Reich, S.; Thomsen, C.; Webster, H. S.; Czerw, R.; Carroll, D. L.; Vieira, S. M. C.; Birkett, P. R.; Rego, C. A. Raman characterization of boron-doped multiwalled carbon nanotubes. *Appl. Phys. Lett.* **2002**, *81*, 2647−2649.

(43) McGuire, K.; Gothard, N.; Gai, P.; Dresselhaus, M.; Sumanasekera, G.; Rao, A. Synthesis and raman characterization of boron-doped single-walled carbon nanotubes. **2005**, *43*, 221−227.

(44) Chou, S. G.; Son, H.; Jorio, A.; Zheng, M.; Dresselhaus, G.; Dresselhaus, M. S. Length characterization of DNA-wrapped carbon nanotubes using Raman spectroscopy. *Appl. Phys. Lett. 88*, l06-07962.

(45) Anderson, N.; Hartschuh, A.; Cronin, S.; Novotny, L. Nanoscale vibrational analysis of single-walled carbon nanotubes. *J. Am. Chem. Soc.* **2005**, *127*, 2533−2537.

(46) Cançado, L. G.; Pimenta, M. A.; Neves, B. R. A.; Dantas, M. S. S.; Jorio, A. Influence of the atomic structure on the raman spectra of graphite edges. *Phys. Rev. Lett.* **2004**, *93*, 247401.